Dynamical formation of microlenses by the reflow method: numerical simulation and experimental study of the process fabrication

2010 J. Micromech. Microeng. 20 095008

(http://iopscience.iop.org/0960-1317/20/9/095008)

J. Micromech. Microeng. **20** (2010) 095008 (9pp) doi:10.1088/0960-1317/20/9/095008

Dynamical formation of microlenses by the reflow method: numerical simulation and experimental study of the process fabrication

Stéphanie Audran[1], **Bénédicte Mortini**[1], **Benoit Faure**[1] **and Guy Schlatter**[2]

[1] STMicroelectronics, 850 rue Jean Monnet, Crolles Cedex 38926, France
[2] Laboratoire d'Ingénierie des Polymères pour les Hautes Technologies (LIPHT EAC 4379), Université de Strasbourg, ECPM, 25 rue Becquerel, Strasbourg Cedex 67087, France

E-mail: stephanie.audran@st.com

Received 23 February 2010, in final form 22 June 2010
Published 5 August 2010
Online at stacks.iop.org/JMM/20/095008

Abstract
In order to study the dynamics of microlens formation by the reflow method, we develop a model based on the Navier–Stokes equation that describes the formation of a microlens from its initial state (photolithographic dot) up to its final shape (rounded microlens). In CMOS imagers, photoresists used to form microlenses contain crosslinkers in order to obtain chemically and thermally stable microlenses at the end of the process. This model takes into account the effect of surface tension as well as the viscosity evolution with bake time, due to the crosslinking reaction. The results of the dynamic modelling show that the microlens passes through different intermediate steps before achieving its expected final spherical shape. It also shows that fast crosslinking kinetics leads to non-spherical microlenses. Indeed the fast increase of viscosity has the effect of blocking the formation of the microlens and freeze the microlens profile in an intermediate shape. Thus, with such type of photoresist materials, contrary to what is reported in the literature, the final shape of the microlens does not depend only on the initial volume or the aspect ratio of the resist pattern. This is the competition, during the melting bake, between the microlens formation under the effect of surface tension and the crosslinking reaction that determines, over all, the final shape that the microlens will adopt.

(Some figures in this article are in colour only in the electronic version)

1. Introduction

The interest in the study of microlens arrays has increased during the past few years due to the wide range of applications of these micro-optical components. Microlenses are commonly used in fibre coupling for optical interconnections and in miniaturized chemical detection systems. In imaging systems, the presence of microlens arrays on the surface of CCD or CMOS image sensors is used to focus the incident light onto the photosensitive area of the pixel, which represents only 30% of the total pixel area [1]. This leads to a significant gain in terms of sensor quantum efficiency (QE), which is defined as the number of electrons generated and collected in a pixel over the number of photons penetrating the pixel. Typically, the presence of microlenses enables us to improve the QE by a factor of 1.4. In this study we have worked on sub-4 μm diameter microlenses.

Among all the techniques used to fabricate microlenses [2–5], the thermal reflow method is probably the most popular because of its simplicity, low cost and high optical performance. This process consists in forming resist patterns using the standard lithographic technique and melting them above the material glass temperature so that surface tension

pushes the resist patterns to adopt a spherical shape. Although the theory predicts the formation of spherical microlenses due to the minimisation of surface energy, experiments show that perfect spherical microlenses are not always achieved [6].

In practice, the microlens shape also depends on the contact angle between the substrate and the resist [7]. This angle is a material property for a particular photoresist/substrate/air combination. It is generally assumed that the resist volume is conserved and that the microlens foot does not move during the melting step. In the case of a large contact angle (as is the case for photoresist on a glass substrate), the slope at the edge of the microlens is rather steep. If there is enough liquid in the initial resist volume, a spherical microlens can be formed. In contrast, if there is not enough liquid available, a dip can be formed in the centre. According to O'Neill and Sheridan [7] there is only one particular volume that will result in a spherical surface for a given lens base width. To obtain spherical microlenses, the photoresist volume for each microlens must be precisely estimated before beginning the thermal reflow process. For a given lens width, the photoresist thickness that should be deposed to achieve a specific microlens height can be evaluated by simple geometrical considerations (volume balance before and after melting) [7]. Therefore, the formation of perfect spherical microlenses would only be possible for specific values of the thickness to width ratio.

But in the case of photoresists used for the CMOS imagers application, the problem is more complex. This comes from the nature of the physicochemical mechanisms involved in the microlens formation. An important phenomenon generally occurs during the microlens process, which also plays a significant role in the final shape of the microlenses: the resist crosslinking reaction [8, 9]. The aim, in using such crosslinkable photoresist materials, is to form thermally and chemically stable microlenses. Indeed, at the end of their process, microlenses become an entire part of the chip, and therefore they should resist not only the thermal budget induced by the operations that follow the microlens formation (chip packaging) but also the external constraints (UV exposition, thermal budget, etc) that the chip will undergo during its lifetime. This crosslinking reaction is generally thermally activated and takes place during the melting bake. Resist crosslinking consists in the formation of covalent bonds between reactive functions present on the polymer chains and on the crosslinking agents. As these binder compounds have functionality superior to 1, this crosslinking reaction leads to the formation of a 3D network, linking the polymer chains with each other, and thus reducing their mobility. As a consequence, the crosslinking of the resist during the melting bake drastically increases the resist viscosity, which hinders the formation of the microlens.

Some studies have been dedicated to the modelling of the final microlens profile. In the work of O'Neill and Sheridan [10, 11], the modelling of the microlens surface is determined analytically using a heuristic polynomial approach. The authors have studied the effect of the deposited layer thickness on the final microlens shape. In the work of Lin *et al* [12], a numerical method is used to predict the thickness of the deposited film to fabricate hexagonal microlens arrays, whereas Schilling *et al* [13] have developed a finite element method based on surface minimization to calculate the 3D surface of microlenses. All these models do not take into account the crosslinking of the resist. Most of the literature related to microlens profiles modelling only presents simulations of the *final* shapes of microlenses manufactured with the reflow method.

In this paper we study the *dynamics* of microlens formation and present a model based on the Navier–Stokes equation that describes the formation of a microlens from its initial up to its final shape. This model takes into account the effect of surface tension as well as the viscosity evolution with bake time, due to the crosslinking reaction. After the description of the model, we first study the thermal behaviour of the photoresist. Then the results of the dynamic modelling of microlens formation are presented and compared with the experimental data. Finally, the influence of some physical parameters (Newtonian viscosity, initial pattern aspect ratio) on the final shape of the microlenses is studied and compared with experiment.

2. Experiments

2.1. Rheological characterization of the photoresist

The rheological characterization of the photoresist was performed on a TA Instrument ARES rheometer in a parallel-plate configuration (diameter = 10 mm, gap = 0.7 mm), using a multiwave temperature ramp test. As the crosslinking temperature of our resist is around 120 °C, for the rheological test, the resist samples were placed between the plates at 100 °C to be sure that no chemical reaction starts before recording the data. Then, as we start the test, a temperature ramp enables us to reach the temperature set point (here 190 °C) within 200 s.

2.2. Microlens fabrication and characterization

The photoresist used in this study was an I-line positive tone photoresist. Its density is $\rho = 1000$ kg m^{-3} and its surface tension $\gamma = 2 \times 10^{-2}$ N m^{-1}. These values are typical for photosensible resists [13, 14]. It was spin-coated on 8 inch silicon wafers and soft-baked in a temperature range of 90–100 °C for 90 s. The wafers were then exposed on an I-line stepper and developed in a basic aqueous solution for 80 s. At the end of this step, resist patterns of 3.6 μm dimension (cf figure 1(*a*)) were obtained. The final process step consists in melting the photoresist patterns on a hot plate at a specific temperature, between 170 °C and 250 °C, for 30 s. During this step the surface tension pulls the melted photoresist patterns into spherical microlenses. But we also know [8, 9] that this hard bake induces resist crosslinking, which is thermally activated. As a consequence, two phenomena arise simultaneously during the final melting bake: the formation of the microlens under the effect of surface tension and the crosslinking of the resist.

In order to study the dynamical evolution of microlens formation, we stopped the melting bake process at different

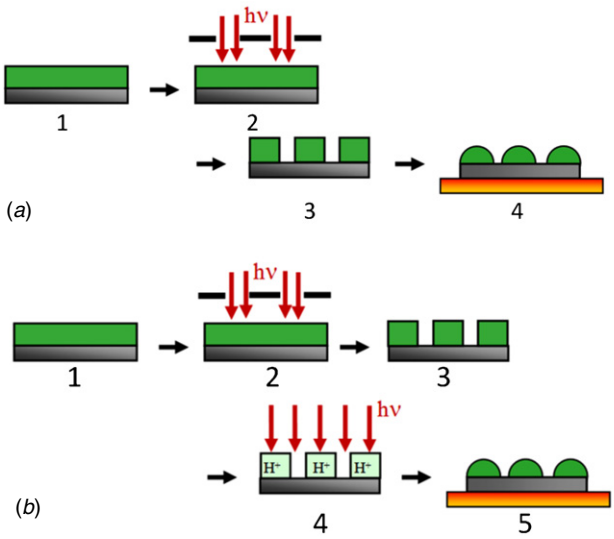

Figure 1. Description of the two processes used to study the effect of crosslinking kinetics: (*a*) 'slow crosslinking kinetics' process; (*b*) 'fast crosslinking kinetics' process.

times ranging from 0 s to 30 s. Six different silicon wafers were used for that purpose. The time of melting bake for each wafer was respectively 0 s (no melting), 2 s, 3 s, 4 s, 5 s and 30 s. After the melting bake, the wafer was finally put in contact with a cold plate.

The measurement of microlens profiles obtained at the different bake times was carried out using atomic force microscopy (AFM) (VEECO, Nanoscope IIIA) in tapping mode.

In order to study the effect of crosslinking kinetics on the final microlens shape, microlenses have been formed with two different processes (figure 1):

(a) the 'slow crosslinking kinetics' process described above that consists in performing a melt bake (MB) directly after the photolithographic steps (coat/exposure/development). In this case, the resist crosslinking reaction that occurs during the MB is only thermally activated.

(b) the 'fast crosslinking kinetics' process that consists in adding a flood exposure step between the photolithographic steps and the MB step. The role of this flood exposure is to generate acid molecules that will catalyze the resist crosslinking reaction that is thermally activated during the MB. As a consequence, the crosslinking kinetics in this process is faster.

Two wafers have been processed with these two different processes. Same dimension of resist pattern (3.6 μm) and same thermal budget have been used in both cases. Characterization of the microlens profile has then been carried out using AFM.

Finally, in order to study the effect of the pattern aspect ratio on microlens formation and compare them to simulation results, wafers have been exposed with an engineering mask containing three different pattern pitches (3.6 μm, 2.6 μm and 1.6 μm).

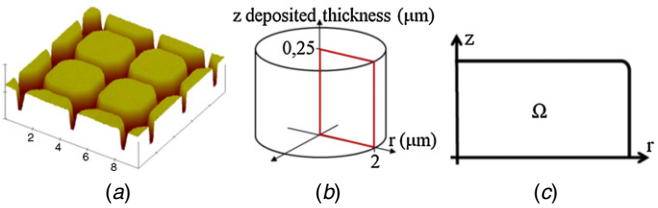

Figure 2. (*a*) AFM picture of the initial shape of resist patterns; (*b*) simplified cylindrical geometry of the model pattern; (*c*) geometry in cylindrical coordinates.

3. Model

Experimentally, our microlenses are made from octagonal patterns. The microlens geometry is assumed to be cylindrical allowing us to reduce the problem to an axisymmetric 2D problem (figure 2).

Over T_g, the resist is assumed to be a viscous incompressible fluid. Thus, neglecting the gravity force due to the very small size of a microlens [15], the hydrodynamic behaviour of this system is governed by the Navier–Stokes and mass conservation equations (equation (1)):

$$\rho \frac{\partial \vec{u}}{\partial t} = -\vec{\nabla} P + \nabla.(\eta \nabla \vec{u}) \tag{1}$$

$$\nabla \cdot \vec{u} = 0, \tag{2}$$

where ρ is the resist density, u the velocity and P the pressure in the microlens. At the microlens free surface, the normal component of the stress results from Laplace's law:

$$\vec{n} \cdot \eta(\nabla \vec{u} + {}^t\nabla \vec{u}) \cdot \vec{n} = P + \frac{\gamma}{R}, \tag{3}$$

where γ is the surface tension of the resist, $\vec{n}$ is the unit vector normal to the surface and R is the local curvature radius of the microlens surface. Furthermore, at the free surface, the tangential component of the stress is assumed to be equal to zero:

$$\vec{t} \cdot \eta(\nabla \vec{u} + {}^t\nabla \vec{u}) \cdot \vec{n} = 0. \tag{4}$$

At the z cylindrical axis, a non-slip condition in the direction perpendicular to the axis is considered, whereas at the bottom of the microlens, the resist is assumed to stick:

$$\vec{n} \cdot \vec{u}_{(r=0)} = 0 \qquad \text{and} \qquad \vec{u}_{(z=0)} = 0. \tag{5}$$

In this study, we are modelling the deformation of a free surface as a function of time. Free surface deformation problems have been widely studied in the literature. A variety of numerical simulations based on the finite element method have been developed by several authors to obtain results in an efficient way. There are two main approaches to compute physical problems involving free surfaces. One approach consists in using a stationary fixed mesh in which the free surface is captured thanks to a specific numerical algorithm. The best-known algorithms are the marker and cell (MAC) method [16, 17], the volume of fluid (VOF) method [18–20] and the level set method [21, 22]. The second approach uses a mesh that can deform and for which the boundaries move with the free surface in a Lagrangian fashion [23–25]. On one hand, these methods are time consuming because the mesh must be

regenerated after each or some time steps. But on the other hand, the free surface is tracked very accurately compared to methods based on fixed mesh. In this work, moving mesh has been used as the computational method for capturing the free surfaces of the microlens. The problem was solved thanks to the Femlab2.3 software.

4. Results and discussion

4.1. Thermal behaviour of the photoresist

As discussed in the introduction, an important phenomenon occurs during our microlens process and more particularly during the melting bake: this is the resist crosslinking reaction. This reaction, which is thermally activated, has the effect of reducing the mobility of polymer chains (i.e. increasing the resist viscosity as the bake time goes on).

In order to take into account this phenomenon in the simulation, we need a law that describes the evolution of viscosity with time: $\eta(t)$. In the first approximation, we have used a linear law.

We have performed some rheological tests on the microlens resist, in order to evaluate the magnitude of the resist viscosity.

- at $t = 0$, i.e. before the MB, at ambient temperature, when resist is not crosslinked but is under its T_g. This viscosity is called η_0.
- at $t_i(T_{\mathrm{MB}})$ which corresponds to the initial time of the MB when the wafer is put in contact with the hotplate set at a temperature in the range of 170–250 °C. This viscosity is called η^i_{TMB}.
- at $t_f(T_{\mathrm{MB}})$ which corresponds to the end of the MB ($t_f = t_i + 30$ s) when the resist is crosslinked. This viscosity is called η^f_{TMB}.

The description of sample preparation for the rheological test has been detailed in a previous paper [9].

From an experimental point of view, it is not possible to reproduce, on the rheometer, the real conditions that the resist undergoes during the microlens process. Indeed, during this process, when the wafer is put in contact with the hotplate, the resist material passes almost instantaneously from ambient temperature to a temperature of around 200 °C. But on the rheometer, the resist sample must be placed between the plates at a temperature inferior to the resist crosslinking temperature; otherwise the material is crosslinked before we can record the data.

As the crosslinking temperature of our resist is around 120 °C, for the rheological test, the resist samples were placed between the plates at 100 °C to be sure that no chemical reaction started before we could register the data. Then, as we started the test, a temperature ramp enabled us to reach the temperature set point (here 190 °C) within 200 s. The evolution of the complex dynamic viscosity η^* as a function of time and temperature is displayed in figure 3.

Figure 3 shows that at $t = 0$ and $T = 100$ °C, the resist viscosity is around 10^4 Pa s. Under the effect of temperature ($T = 124$ °C and $t = 77$ s), the resist viscosity decreases to a value of 2×10^2 Pa s and for $t > 77$ s and $T > 124$ °C,

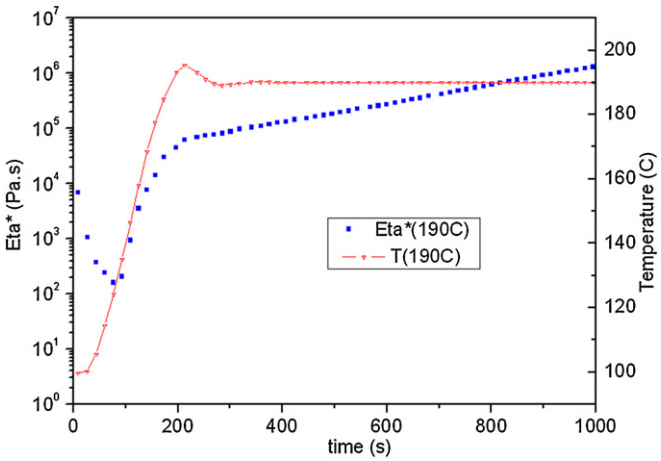

Figure 3. Evolution of microlens resist viscosity as a function of time and temperature ($\omega = 0.78$ rad s^{-1}).

Table 1. Resist viscosity value reached at the end of the MB by varying the slope of the linear law and used in the simulation to study the effect of crosslinking kinetics on the final microlens shape.

λ: slope of the linear law	η^f_{TMB} (Pa s)
50	1 700
100	3 200
200	6 200
300	9 200
500	15 200

the viscosity increases due to resist crosslinking. In only 30 s (typical duration of the MB in our microlens process), and by increasing the temperature by 20 °C, the viscosity increases by almost one decade. Indeed $\eta^* \sim 10^3$ Pa s at $t = 109$ s and $T = 146$ °C.

In our process, the resist is instantaneously put in contact with a hotplate set at around 200 °C. As a consequence, the resist viscosity at t_i(200 °C) must be inferior to 2×10^2 Pa s, and the viscosity at t_f(200 °C) must be much higher than 10^3 Pa s.

In further numerical simulations, we have considered that

- at $t = 0$, $\eta_0 = 1500$ Pa s
- at $t_i(T_{\mathrm{MB}})$, $\eta^i_{\mathrm{TMB}} = 200$ Pa s
- at $t_f(T_{\mathrm{MB}})$, η^f_{TMB} reaches different values depending on the slope of the linear law (cf table 1). As we will see in section 4, varying the slope of the linear law $\eta(t)$ has enabled us to study the effect of resist crosslinking kinetics on the microlens shape obtained at the end of the MB.

The linear law used in the simulation to describe the increase of resist viscosity due to resist crosslinking is arbitrary and does not correspond to what happens in reality. As a consequence, the time scale of the modelling must not be compared to the experiment. The purpose of this modelling is to over all describe the different steps through which the microlens passes during its formation. Future work to improve this model would be to determine an experimental law describing the evolution of resist viscosity with time and temperature to really reproduce what occurs during our process.

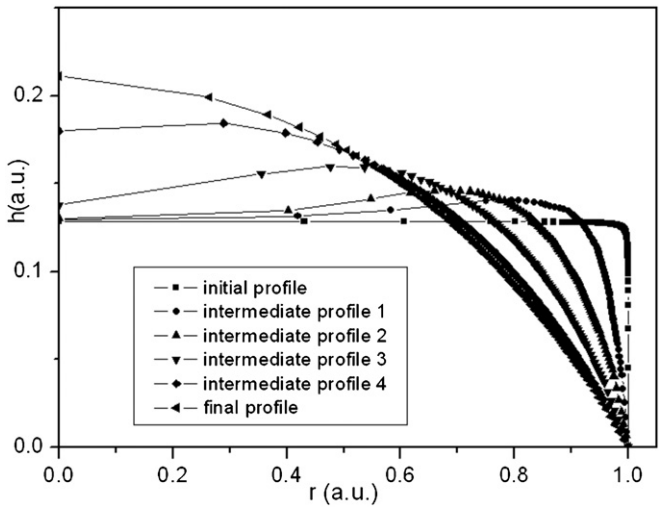

Figure 4. Modelling of the microlens profile evolution from its initial cylindrical shape to its final hemispherical shape.

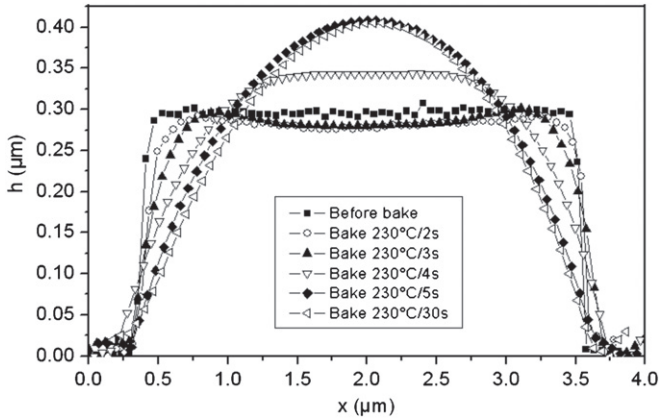

Figure 5. AFM measurements of the dynamical formation of the microlens shape.

4.2. Dynamic microlens formation

We have simulated the evolution of the microlens profile during its formation with $\eta^{f}_{\mathrm{TMB}} = 1700$ Pa s, which corresponds to a slope $\lambda = 50$. Figure 4 shows the evolution of the microlens profile from its initial rectangular shape to its final spherical shape, described by the model. Figure 4 shows that first a small bump is formed at the edge of the resist pattern, which gives the microlens a kind of volcano shape. Then, this bump is propagating like a wave from the edge to the centre of the resist pattern, to give an intermediate flat profile, and to finally form a spherical dome.

In order to check the validity of the model, numerical simulations have been compared to the experimental data. The different states through which the microlens passes during its formation were observed by stopping the melting bake at different intermediate times as described in section 2. The AFM profiles of the microlenses obtained at the different bake times are shown in figure 5. For a better visualization of the phenomenon, three-dimensional AFM images are presented in figure 6. It is shown that after only 2 s of bake, the edge of the resist pattern becomes rounded and the central height of the pattern slightly decreases. After 4 s, the resist material has moved from the edge to the central region, forming an intermediate flat microlens. Finally, we see that after 5 s of bake, the microlens has almost achieved its final spherical shape. Indeed, the profiles at $t = 5$ s and $t = 30$ s are nearly the same.

Thus, results obtained from the model are in agreement with the experiment. Indeed, we find the same intermediate steps of the microlens formation: the microlens passes through a volcanic shape, then an intermediate flat profile, to finally form a spherical cap. Moreover, an important assumption of the modelling is validated in this experimental case: the contact between the foot of the microlens and the substrate is sticky. Indeed, experimental results show that there is almost no slipping of the microlens foot on the substrate.

4.3. Effect of crosslinking kinetics

The influence of the kinetics of resist crosslinking on the final shape of the microlens is studied. As previously explained, in order to take into account the resist crosslinking that occurs during the microlens formation, we have considered in the first approximation that the resist viscosity varied linearly with the bake time. Figure 7 shows the final microlens profile obtained as the slope λ of the viscosity law varies from 100 to 500 (cf table 1).

This result shows that, as the crosslinking kinetics becomes faster, the final profile of the microlens deviates from the spherical case. The fast increase of viscosity has for effect to block the formation of the microlens and freeze the microlens profile in an intermediate step. Indeed, we obtain a flat profile for $\lambda = 200$ and a volcanic profile for $\lambda = 500$.

In order to experimentally observe the influence of the resist crosslinking kinetics on the final microlens shape, we fabricated microlenses with the two different processes described in section 2 (i.e. the 'low crosslinking kinetics' process and the 'fast crosslinking kinetics' process). Figure 8 shows the final microlens profile obtained with the two different processes. In both processes, the bake temperature is the same (190 °C).

It is shown that the 'fast crosslinking kinetics' process leads to the formation of a microlens with a cavity at the centre (volcano shape), whereas the 'slow crosslinking kinetics' process leads to a well formed microlens. This result confirms the numerical simulation. Thus, during the bake, two phenomena occur simultaneously: the formation of the microlens under the effect of surface tension and the crosslinking of the resist. However, these two phenomena have opposite effects:

(i) surface tension minimizes the microlens area by pushing it towards a spherical surface.

(ii) the crosslinking reaction, in contrast, has the effect of linking the polymer chains with each other, and consequently decreasing their mobility, which hinders the formation of the microlens. Indeed, the resist glass transition temperature T_g increases with the crosslinking reaction, and when T_g becomes superior to the temperature of the MB, the resist reflow is no longer possible.

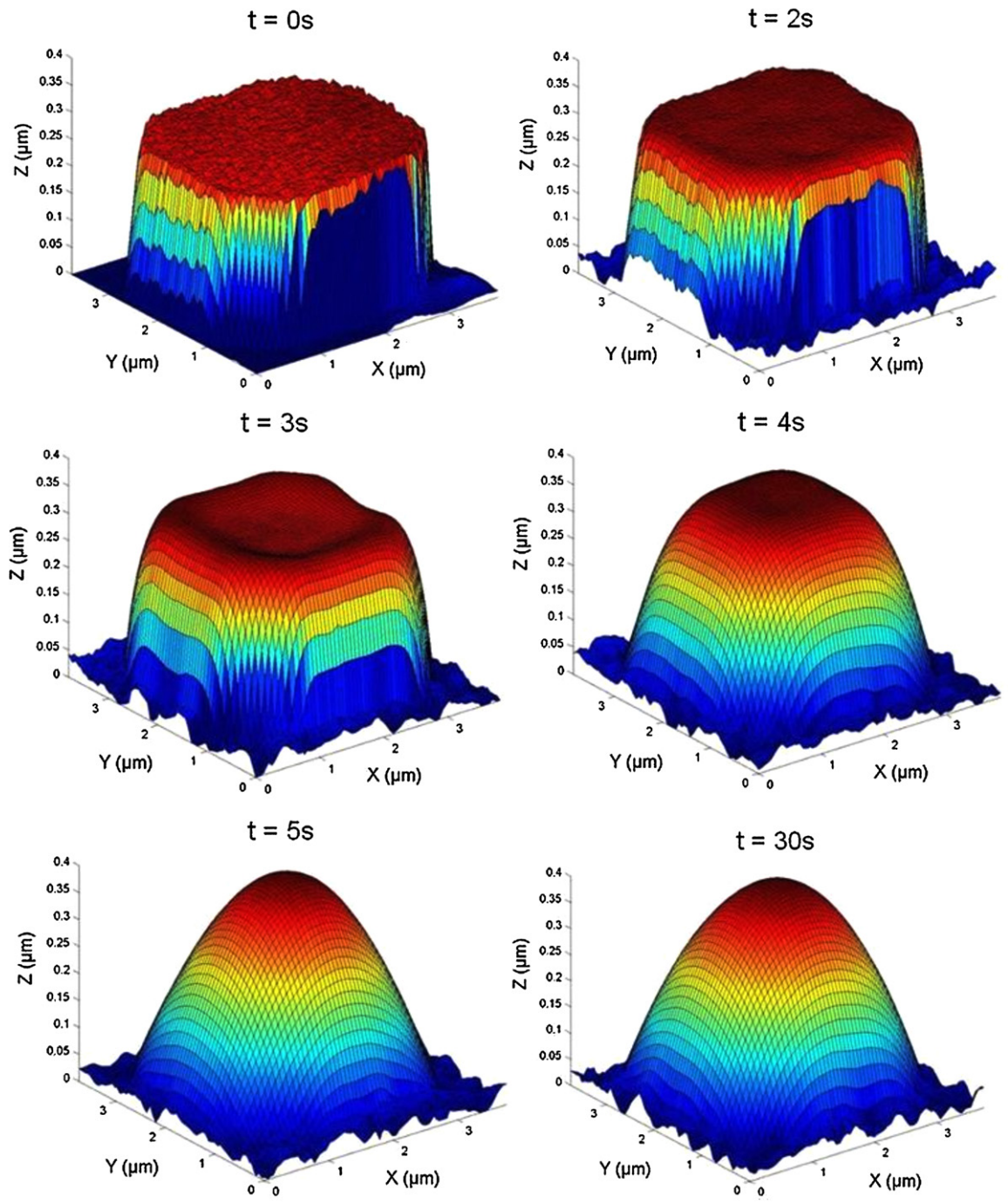

Figure 6. Three-dimensional views of microlens AFM profiles obtained after different bake times ($t = 0$ s, 2 s, 3 s, 4 s, 5 s and 30 s).

If the resist crosslinking kinetics is too fast, it will freeze the polymer chains before the surface tension has transformed the resist pattern into a spherical microlens. This is what we observe experimentally with the 'fast crosslinking kinetics' process: the microlens profile is blocked in an intermediate step of its formation.

Thus, we claim that in order to correctly form the microlens, it is not enough to choose a bake temperature superior to the initial T_g of the resist, but it is necessary to take into consideration both the kinetics of microlens formation and the resist crosslinking kinetics. Moreover, in contrast to what is reported by O'Neill and Sheridan [7], in the case of crosslinkable material, the initial volume of the resist pattern does not determine by itself the final shape of the microlens. The initial pattern volume determines the shape at the thermodynamical equilibrium but not the final shape that depends in this case on the kinetics of resist crosslinking and microlens formation.

4.4. Effect of aspect ratio

We also studied the influence of the aspect ratio of the resist pattern on the final shape of the microlens. The aspect ratio k

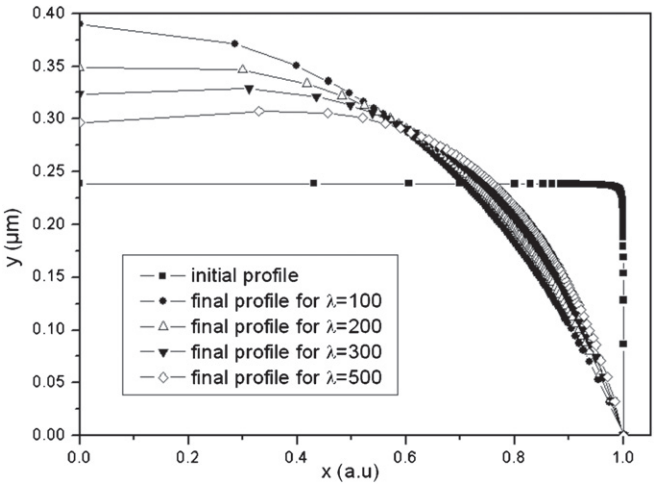

Figure 7. Final profiles of microlenses obtained for different kinetics of viscosity increase.

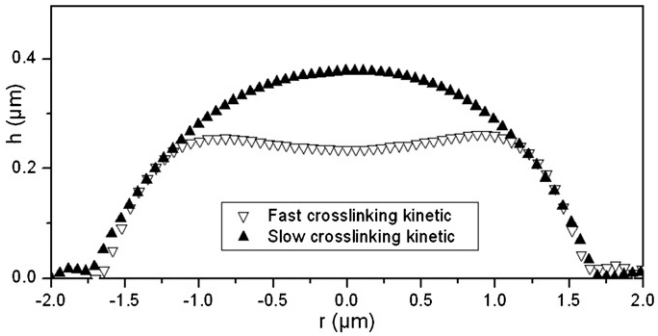

Figure 8. AFM microlens profile obtained with the 'fast crosslinking kinetics' process (the crosslinking reaction activated during the bake is catalyzed) and the 'slow crosslinking kinetics' process (the crosslinking reaction is only thermally activated).

of the resist pattern is defined as the ratio between the pattern thickness and its diameter:

$$k = \frac{t}{d}, \tag{6}$$

where t is the resist pattern initial thickness and d is the resist pattern diameter. According to Nussbaum *et al* [26], there is a minimum value of k equal to 0.04 at which the final microlens is not well formed and presents a dip in the centre. According to the authors, this result should be due to an incomplete melting of the resist drop, especially in the case of large and flat microlenses. For large resist volumes, the outer part of the liquid drop might already be crosslinked before the inner part is completely melted. Daly *et al* [6] have also observed that at a low aspect ratio, the melting process merely rounds the edges of the pattern but does not produce an overall circular shape. According to them, at a low aspect ratio, the surface tension of the melted resist is not sufficient to draw the material into the desired shape.

In order to study the influence of the pattern aspect ratio on the final microlens shape we have used three dimensions of the pattern designed into our engineering mask: 1.6 μm, 2.6 μm and 3.6 μm microlens. The respective aspect ratios of these patterns associated with a film thickness of 160 nm

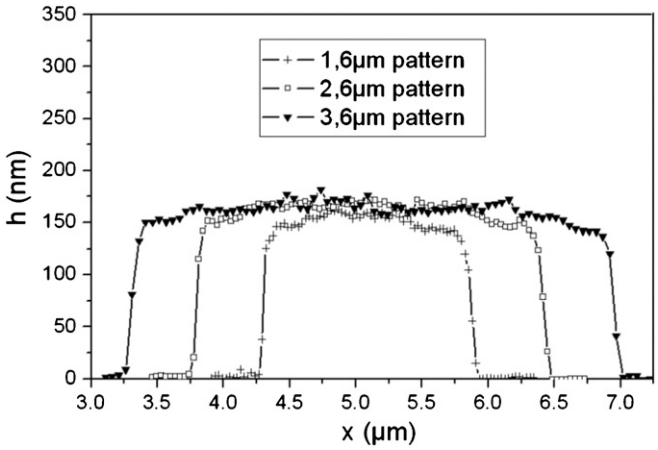

Figure 9. AFM profiles of the initial resist pattern of base: 1.6 μm, 2.6 μm and 3.6 μm.

Table 2. Aspect ratio of the three resist patterns used to form the microlenses.

Pattern diameter	Aspect ratio k
1.6 μm	0.1
2.6 μm	0.06
3.6 μm	0.04

are presented in table 2 and their AFM scans are presented in figure 9.

As we can notice, the aspect ratio of the 3.6 μm pattern corresponds to the minimum value under which, according to Nussbaum *et al* [26], the microlens presents some shape issues. Microlenses have then been formed by using the 'fast crosslinking kinetics' and the 'slow crosslinking kinetics' processes at the same bake temperature of 230 °C. The AFM profiles of the microlenses obtained from the different patterns with the two different processes are presented in figures 10(*a*) and (*b*).

Figure 10(*a*) shows that with the 'fast crosslinking kinetics' process,

- the 1.6 μm-based microlens is well formed,
- the 2.6 μm-based microlens presents a rather flat profile and
- the 3.6 μm-based microlens presents a volcanic profile with a dip in its centre.

On the other hand, figure 10(*b*) shows that whatever the initial dimension of the resist pattern, all the microlenses formed with the 'slow crosslinking kinetics' process are well formed.

In the previous section, we have seen that fast reaction kinetics has the effect of freezing the shape of the microlens in an intermediate state of its formation. This is what we observe for the microlenses of base 2.6 μm and 3.6 μm, obtained with the 'fast crosslinking kinetics' process, which respectively present a flat profile and a volcano shape. On the other hand, the 1.6 μm microlens is well formed. One explication could be that the formation of the 1.6 μm microlens is faster than that of the 2.6 μm and 3.6 μm microlenses. As a consequence, the 1.6 μm microlens has the time to reach

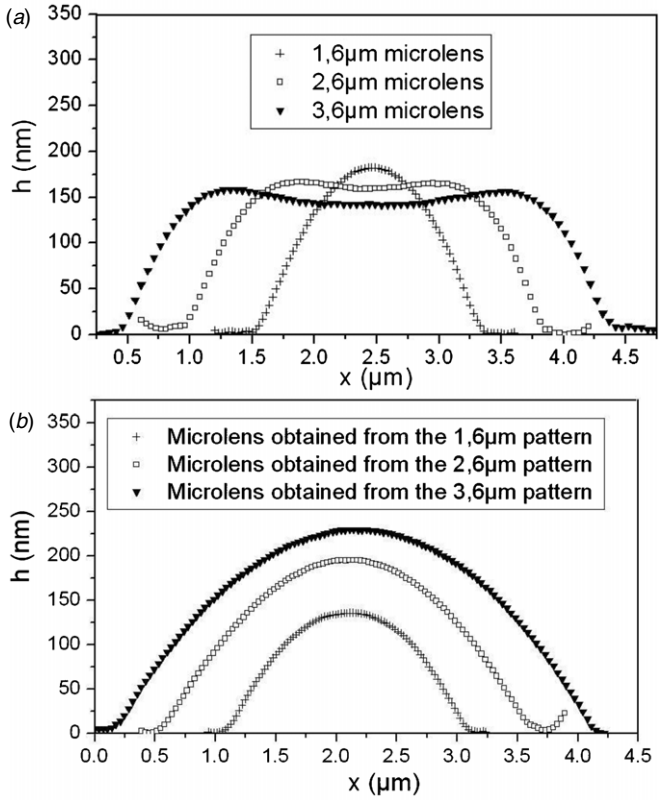

Figure 10. Microlenses obtained from the different pattern dimensions with (*a*) the 'fast crosslinking kinetics' process and (*b*) the 'slow crosslinking kinetics' process.

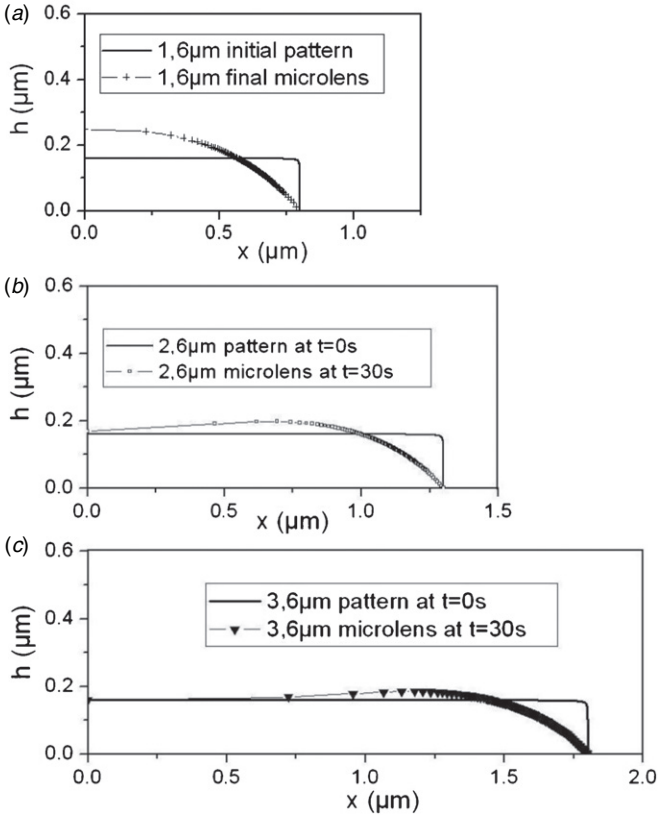

Figure 11. Simulated profiles at the end of the process for radius: (*a*) 0.8 μm (1.6 μm base); (*b*) 1.3 μm (2.6 μm base); (*c*) 1.8 μm (3.6 μm base).

its spherical equilibrium shape before the resist crosslinking has totally frozen the mobility of the polymer chains (which is not the case for the 2.6 μm and 3.6 μm microlenses). The shapes of the 2.6 μm and 3.6 μm microlenses also confirm this hypothesis because the state at which the formation of the 2.6 μm microlens has been stopped (flat microlens) is more advanced than that of the 3.6 μm microlens (volcano shape).

In order to verify this hypothesis, we have simulated the final microlens profile of three microlenses obtained from three pattern dimensions equivalent to those used in the experiment with $\eta^{f}_{\mathrm{TMB}} = 1700$ Pa s corresponding to a slope $\lambda = 50$. The respective radii and the thickness of the three patterns considered in the simulation are $r_1 = 0.8$ μm, $r_2 = 1.3$ μm, $r_3 = 1.8$ μm and $t = 0.16$ μm. The results of the final microlens profiles obtained from the three pattern dimensions are presented in figure 11.

These results show that after an identical simulation time, the 1.6 μm microlens has almost achieved its spherical shape whereas the 2.6 μm microlens is only in an intermediate step of its formation (volcano profile) and the 3.6 μm is also in an intermediate step that is even less advanced. As a consequence, the simulation results confirm that, for a given pattern thickness, the larger the pattern base, the slower the formation of the microlens.

If we consider the results obtained with the 'slow crosslinking kinetics' process, we see that the microlenses are well formed whatever the dimension of the initial pattern. In this process, the crosslinking kinetics is slower because the reaction is not catalyzed. As a consequence, the microlenses have the time to reach their equilibrium shape before the progress of the crosslinking reaction reaches the point at which the mobility of the polymer chains is frozen.

Thus, in the case of crosslinkable materials, the final shape of the microlens is not determined only by the initial volume or the aspect ratio of the resist pattern. We have demonstrated that for the same pattern geometry (volume and aspect ratio) and for identical bake conditions, we can obtain totally different results depending on the crosslinking reaction kinetics. As a consequence, this is the competition between the microlens formation under the effect of surface tension and the crosslinking reaction that determines, over all, the final shape that the microlens will adopt.

5. Conclusion

Microlens arrays formed by the reflow method are commonly used in CMOS image sensors to improve the sensor quantum efficiency. In such applications, crosslinkable resists are used in order to form thermally and chemically stable microlenses that become an entire part of the final chip. The resist crosslinking occurs simultaneously with the resist melting during a hard bake step. The purpose of this paper was to study the dynamics of microlens formation and to identify the root cause of non-spherical microlenses observed under certain conditions. The study has been made on sub-4 μm diameter microlenses.

The numerical simulation developed in this work and based on the Navier–Stokes equation has enabled us to describe the intermediate steps of microlens formation and the impact of crosslinking kinetics on the final microlens shape. Simulated results have been compared to experimental data and clear correlations have been demonstrated allowing us to explain the experimental microlens shape. The specificity of the reflow method is that two phenomena occur simultaneously during the microlens process: the microlens formation under the effect of surface tension and the resist crosslinking that increases resist viscosity. If crosslinking reaction kinetics dominates, the microlens shape is blocked in an intermediate step of its formation, which leads to non-spherical microlenses. If the microlens formation kinetics predominates, the equilibrium shape can be achieved, which leads to well-formed microlenses.

Thus, the final shape of the microlens is not only determined by the initial volume or the aspect ratio of the resist pattern, but over all by the competition between the effect of surface tension and the effects of crosslinking reaction. The right tuning of the process conditions (MB temperature and additional steps) seems to be the key parameter in the control of the final microlens shape because it enables us to adjust the kinetics of each mechanism, and thus favour the microlens formation with regard to resist crosslinking.

References

[1] Fan Y T, Peng C-S and Chu C-S 2000 Advanced microlens and color filter process technology for the high efficiency CMOS and CCD image sensor *Proc. SPIE* **4115** 263–74

[2] Hartmann D M, Kibar O and Esener S C 2000 Polymer microlens arrays fabricated using the hydrophobic effect *Proc. SPIE* **4089** 496–507

[3] Ong N S, Koh Y H and Fu Y Q 2002 Microlens array produced using hot embossing process *Microelectron. Eng.* **60** 365–79

[4] Yao J, Cui Z, Gao F, Zhang Y, Guo Y, Du C, Zeng H and Qiu C 2001 Refractive microlens array made of dichromate gelatine with gray-tone photolithography *Microelectron. Eng.* **57–58** 729–35

[5] Lee S-K, Lee K-C and Lee S S 2002 A simple method for microlens fabrication by the modified LIGA process *J. Micromech. Microeng.* **12** 334–40

[6] Daly D, Stevens R F, Hutley M C and Davies N 1990 The manufacture of microlenses by melting photoresist *Meas. Sci. Technol.* **1** 759–66

[7] O'Neill F T and Sheridan J T 2002 Photoresist reflow method of microlens production: part I. Background and experiments *Optik* **113** 391–404

[8] Audran S, Faure B, Mortini B, Regolini J, Schlatter G and Hadziioannou G 2006 Study of mechanisms involved in photoresist microlens formation *J. Micro. Eng.* **83** 1087–90

[9] Audran S *et al* 2006 Study of dynamical formation and shape of microlenses formed by the reflow method *Proc. SPIE* **6153** 61534D

[10] O'Neill F T and Sheridan J T 2002 Photoresist reflow method of microlenses production: part II. Analytic models *Optik* **113** 405–19

[11] O'Neill F T, Walsh C R and Sheridan J T 2004 Photoresist reflow method of microlens production: modeling and fabrication techniques *Proc. SPIE* **5456** 197–208

[12] Lin C-P, Yang H and Chao C-K 2003 Hexagonal microlens array modeling and fabrication using thermal reflow process *J. Micromech. Microeng.* **13** 775–81

[13] Schilling A, Mertz R, Ossmann C and Herzig H P 2000 Surfaces profiles of reflow microlenses under the influence of surface tension and gravity *Opt. Eng.* **39** 2171–6

[14] Wu S 1970 Surface and interfacial tensions of polymer melts: II. Poly(methyl methacrylate), poly(n-butyl methacrylate), and polystyrene *J. Phys. Chem.* **74** 632–8

[15] Wu S 1982 *Polymer Interface and Adhesion* (New York: Dekker) p 67 chapter 3

[16] Harlow F H and Welch J E 1965 Numerical calculation of time-dependent viscous incompressible flow of fluid with free surface *Phys. Fluids* **8** 2182–9

[17] Nakayama T and Mori M 1996 An Eulerian finite element method for time-dependent free surface problems in hydrodynamics *Int. J. Numer. Methods Fluids* **22** 175–94

[18] Hirt C W and Nichols B D 1981 Volume of fluid (VOF) method for the dynamics of free boundaries *J. Comput. Phys.* **39** 201–25

[19] Shin S and Lee W I 2000 Finite element analysis of incompressible viscous flow with moving free surface by selective volume of fluid method *Int. J. Heat Fluid Flow* **21** 197–206

[20] Yang A-S, Yang J-C and Hong M-C 2006 Droplet ejection study of a Picojet printhead *J. Micromech. Microeng.* **16** 180–8

[21] Osher S and Fedkiw R P 2001 Level set methods: an overview and some recent results *J. Comput. Phys.* **169** 463–502

[22] Chessa J and Belytschko T 2003 An enriched finite element method and level sets for axisymmetric two-phase flow with surface tension *Int. J. Numer. Methods Eng.* **58** 2041–64

[23] Tourigny Y and Hulsemann F 1998 A new moving mesh algorithm for the finite element solution of variational problems *SIAM J. Numer. Anal.* **35** 1416–38

[24] Tezduyar T E, Behr M and Liou J 1992 A new strategy for finite element computations involving moving boundaries and interfaces—the DSD/ST procedure: I. The concept and the preliminary numerical tests *Comput. Methods Appl. Mech. Eng.* **94** 339–51

[25] Koobus B and Farhat C 1999 Second-order time-accurate and geometrically conservative implicit schemes for flow computations on unstructured dynamic meshes *Comput. Methods Appl. Mech. Eng.* **170** 103–29

[26] Nussbaum Ph, Völkel R, Herzig H P, Eisner M and Haselbeck S 1997 Design, fabrication and testing of microlens arrays for sensors and microsystems *Pure Appl. Opt.* **6** 617–36